

# Band gap and band parameters of InN and GaN from quasiparticle energy calculations based on exact-exchange density-functional theory

P. Rinke,<sup>1</sup> A. Qteish,<sup>2</sup> M. Winkelnkemper,<sup>1,3</sup> D. Bimberg,<sup>3</sup> J. Neugebauer,<sup>4</sup> and M. Scheffler<sup>1</sup>

<sup>1</sup>*Fritz-Haber-Institut der Max-Planck-Gesellschaft, Faradayweg 4–6, D-14195 Berlin, Germany*

<sup>2</sup>*Department of Physics, Yarmouk University, 21163-Irbid, Jordan*

<sup>3</sup>*Institut für Festkörperphysik, Technische Universität Berlin, Hardenbergstraße 36, D-10623 Berlin, Germany*

<sup>4</sup>*Max-Planck-Institut für Eisenforschung, Department of Computational Materials Design, D-40237 Düsseldorf, Germany*

(Dated: March 23, 2022)

We have studied the electronic structure of InN and GaN employing  $G_0W_0$  calculations based on exact-exchange density-functional theory. For InN our approach predicts a gap of 0.7 eV. Taking the Burnstein-Moss effect into account, the increase of the apparent quasiparticle gap with increasing electron concentration is in good agreement with the observed blue shift of the experimental optical absorption edge. Moreover, the concentration dependence of the effective mass, which results from the non-parabolicity of the conduction band, agrees well with recent experimental findings. Based on the quasiparticle band structure the parameter set for a  $4 \times 4$   $\mathbf{k} \cdot \mathbf{p}$  Hamiltonian has been derived.

PACS numbers: 71.15.Mb, 71.20.Nr, 78.20.Bh

The group III-nitrides AlN, GaN and InN and their alloys have become an important class of semiconductor materials, in particular for use in optoelectronic devices such as green and blue light emitting diodes (LEDs) and lasers. Among the three materials InN is still the least explored, due to difficulties in synthesizing high quality single crystals. Only very recently these problems have been overcome [1], but many of the key band parameters have not been conclusively determined until now [1, 2]. The most controversially discussed parameter is currently still the fundamental band gap of InN. For many years it was believed to be approximately 1.9 eV, but essentially any value between 0.65 and 2.3 eV has been reported in the literature over the last 30 years [1]. However, more recent experiments on high quality samples grown by molecular beam epitaxy (MBE) and recent *ab initio* calculations support a significantly lower value around 0.7 eV [3, 4, 5, 6, 7].

Different hypotheses have been proposed to explain the large variation in the measured band gaps. Defects could be responsible for inducing states in the band gap or give rise to a pronounced Burnstein-Moss effect due to a shift in the Fermi level caused by a high intrinsic electron density. Non stoichiometry may increase the defect concentration or alter the crystalline structure. The formation of oxides and oxynitrides would increase the band gap, whereas the precipitation of In clusters leads to additional features in optical absorption spectra [1, 8]. In this article we demonstrate that first principles calculations can contribute to the solution of this fundamental question. By combining density-functional theory (DFT) with many-body perturbation theory in the  $G_0W_0$  approximation [9], which is currently the method of choice for calculating quasiparticle excitations in solids [10, 11], we combine atomistic control over the material with accurate calculations for the band structure and the band gap of stoichiometric and defect free structures.

Previous *ab initio* studies were aggravated by the fact that DFT calculations in the local-density approximation (LDA) predict InN to be metallic in the zinc blende and wurtzite structures. Subsequent  $G_0W_0$  calculations only open the gap to 0.02 - 0.05 eV [12, 13], while adding

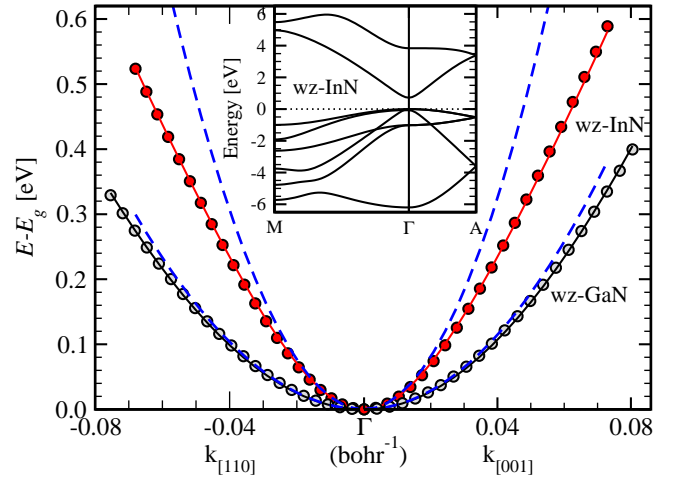


FIG. 1: Conduction band of wurtzite InN and GaN aligned at the bottom of the conduction band: the circles are the  $G_0W_0$  results, the solid lines the  $\mathbf{k} \cdot \mathbf{p}$  fit using Eq. 1, and the dashed lines the effective mass band. The inset shows the band structure of wurtzite InN.

self-interaction corrections to the DFT calculations, either in the screened-exchange [6], exact-exchange optimized effective potential approach (OEPx) [14], or self-interaction corrected (SIC) LDA approach [15, 16], yield a semiconductor with a band gap of 0.8, 1.0 and 1.6 eV for the wurtzite phase, respectively. Here we apply the  $G_0W_0$  corrections to OEPx ground state calculations, which are fully self-interaction free. We have previously shown that this approach yields band gaps for II-VI compounds and GaN in very good agreement with experiment [11] and for wurtzite InN our value of 0.7 eV (see Tab. I) strongly supports the recent experimental findings [3, 4, 5]. Similar conclusions were drawn from previous  $G_0W_0$  calculations applied to SIC-LDA ground states, however, only after adjusting the  $pd$  repulsion and combining calculations with and without the  $4d$  electrons in the core of the In pseudopotential [7, 17].

The OEPx calculations in the present work were performed with the plane-wave, pseudopotential code

param. unit	$a_0$ Å	$c_0$ Å	$u$	$E_g$ eV	$\Delta_1$ eV
zb-GaN	4.50			3.07	
zb-InN	4.98			0.53	
wz-GaN	3.181	5.166	0.377	3.32	0.029
wz-InN	3.533	5.693	0.379	0.72	0.067

TABLE I: Lattice parameters,  $G_0W_0$  band gap  $E_g$ , crystal field splitting  $\Delta_1$  for zinc blende (zb) and wurtzite (wz) GaN and InN.

`sfhngx` [18], while for the  $G_0W_0$  calculations we have employed the  $G_0W_0$  space-time method [19] in the `gwst` implementation [20, 21]. Exact-exchange pseudopotentials [22] were used throughout and the cation  $d$ -electrons were included explicitly [11, 14]. The calculations were performed at the experimental lattice constants [23] taken from Ref. [24] and reported in Tab. I. Convergence to within 0.05 eV in the quasiparticle energies was achieved for a  $4 \times 4 \times 4$  ( $4 \times 4 \times 2$ )  $\mathbf{k}$ -point sampling in the zinc blende (wurtzite) phase and a plane-wave cutoff of 75 (65) Ry for GaN (InN). Unoccupied bands up to 55 (45) Ry were included in the calculation of the polarizability for GaN (InN) in the OEPx as well as in the  $G_0W_0$  calculations.

The  $G_0W_0$  band gap  $E_g$  and the crystal field splitting  $\Delta_1$  for zinc blende and wurtzite GaN and InN are shown in Tab. I. Since  $G_0W_0$  falls into the realm of perturbation theory it is not *a priori* clear if the quasiparticle corrections are positive or negative. While LDA based  $G_0W_0$  calculations generally open the band gap from the underestimated LDA value we observe here that the OEPx gap of 1.0 eV for wz-InN closes to 0.72 eV after applying the  $G_0W_0$  corrections. This is not unexpected since the dielectric screening inherent to  $G_0W_0$  but not to OEPx counteracts the exchange effects.

Figure 1 shows the  $G_0W_0$  bandstructure for wurtzite InN and the conduction band of wurtzite InN and GaN (circles). To make contact with experimental results we use an analytic expression for the conduction band around the  $\Gamma$ -point

$$E_c(k) = \frac{\hbar^2 k^2}{2m_0} + \frac{1}{2} \left( E_g^+ + \sqrt{(E_g^-)^2 + 4E_p \frac{\hbar^2 k^2}{2m_0}} \right), \quad (1)$$

derived from a four band  $\mathbf{k} \cdot \mathbf{p}$  model, neglecting spin-orbit splitting. Here  $m_0$  is the free electron mass and  $E_g^\pm = E_g \pm \Delta_1$ . The parameter  $E_p$  is related to the optical matrix elements between conduction and valence bands. Since it is the only unknown in Eq. 1 it has been determined by fitting to the  $G_0W_0$  conduction band. The small reciprocal lattice vector spacing required for an accurate fit is easily realised in the  $G_0W_0$  space-time method [19] by means of Fourier interpolation [20].

Using the values of Table I for  $\Delta_1$  and  $E_g$  we find that the quasiparticle conduction band of InN is well described by Eq. 1 and  $E_p^\parallel = E_p^\perp = 9.0$  eV (red solid line in Fig. 1). For GaN the transition matrix elements differ for different directions and we obtain  $E_p^\parallel = 14.9$  eV along the  $c$ -axis and  $E_p^\perp = 13.6$  eV in the basal plane (black solid line).

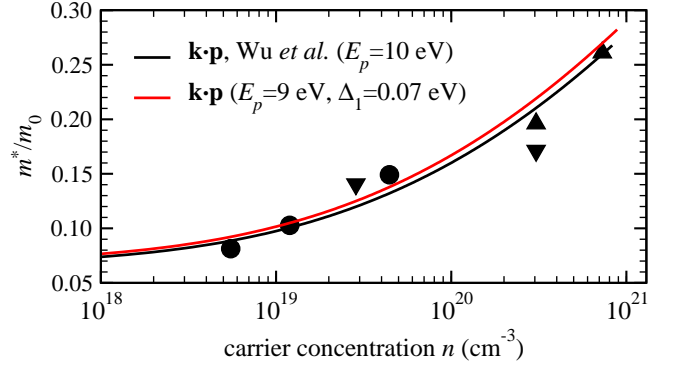


FIG. 2: For wz-InN the effective mass as a function of carrier concentration, deduced from the  $G_0W_0$  calculations by means of Eq. 1 and 2 (red line), agrees well with experimental measurements (symbols) and the  $\mathbf{k} \cdot \mathbf{p}$  fit of Wu *et al.* (black line) based on the experimental data [25, 26]. (Figure adapted from [26])

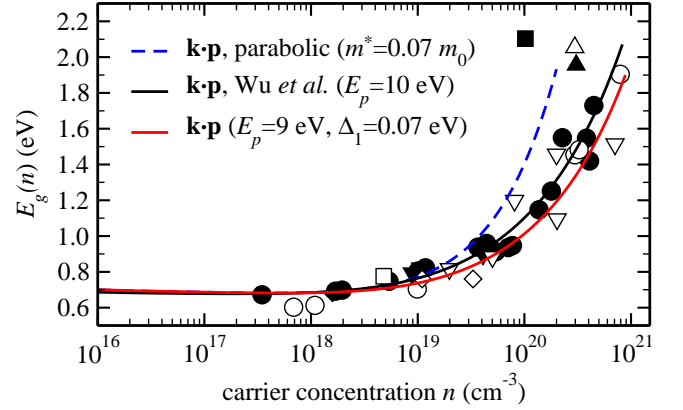


FIG. 3: The Burnstein-Moss effect deduced from the  $G_0W_0$  band structure (red line) for wz-InN reproduces the experimental trend (symbols) very well and is also close to the  $\mathbf{k} \cdot \mathbf{p}$  curve of Wu *et al.* (black line) [25, 26]. Assuming parabolic bands (dashed line) overestimates the Burnstein-Moss shift. (Figure adapted from Ref. [8]; the following symbols differ: • [26] ◇ [27] △ [28])

While the conduction band is well described in the effective mass approximation for GaN (blue dashed lines in Fig. 1) it exhibits a deviation from the parabolic shape in InN. Wu *et al.* have recently reported a dependence of the conduction band effective mass on the free carrier concentration in InN [25, 26], which indicates a pronounced non-parabolicity of the conduction band. In the spherical band approximation the momentum effective mass

$$\frac{m^*(k_F)}{m_0} = \left( \frac{m_0}{\hbar^2 k_F} \frac{dE_c(k)}{dk} \bigg|_{k=k_F} \right)^{-1} \quad (2)$$

can be translated into a carrier concentration dependent effective mass using the free electron relation  $k_F = (3\pi^2 n)^{1/3}$ , where  $n$  is the density of electrons in the conduction band [25, 26]. Figure 2 shows the effective mass of wurtzite InN as a function of the free carrier concentration. The *ab initio* prediction (red line) extracted from

parameter unit	$m_{\perp}^*$ ( $m_0$ )	$m_{\parallel}^*$ ( $m_0$ )	$A_1/\gamma_1$	$A_2/\gamma_2$	$A_3/\gamma_3$	$A_4$	$A_5$	$A_6$	$A_7$ (eVÅ)	$E_p^{\perp}/E_p$ (eV)	$E_p^{\parallel}$ (eV)
zb-GaN	0.193		2.506	0.636	0.977					16.86	
zb-InN	0.054		6.817	2.810	3.121					11.37	
wz-GaN	0.212	0.190	-5.798	-0.545	5.259	-2.473	-2.491	-3.143	0.049	16.22	17.39
wz-InN	0.071	0.067	-15.230	-0.520	14.673	-7.012	-6.948	-9.794	0.174	8.89	8.97

TABLE II: Conduction band effective masses  $m^*$ , Luttinger ( $\gamma_1$ - $\gamma_3$ ) and  $A$  parameters as well as values for  $E_p$  (zinc blende) and  $E_p^{\perp}$  and  $E_p^{\parallel}$  (wurtzite) [29] for GaN and InN obtained by fitting a  $4 \times 4$   $\mathbf{k} \cdot \mathbf{p}$  Hamiltonian to the  $G_0W_0$  band structure.

our  $G_0W_0$  band structure by means of Eq. 1 and 2 reproduces the experimental results very well and closely matches the curve obtained by Wu *et al.* with an experimentally deduced value of  $E_p=10$  eV [25, 26] (black line).

Equation 1 can also be used to calculate the shift of the direct optical transitions ( $E_g(n) = E_c(n) - E_v(n)$ ) towards higher energies in absorption measurements upon increasing electron concentration in the conduction band – the so called Burnstein-Moss effect. Contributions from the electron-ion and electron-electron repulsion at high electron concentrations are accounted for following Wu *et al.* [25, 26]. The Burnstein-Moss shift calculated in this way fits a wide range of experimentally reported measurements very well, as shown in Fig. 3, and agrees well with the curve deduced by Wu *et al.* from their experimentally determined values of  $E_g$  and  $E_p$ . Neglecting the non-parabolicity of the conduction band (blue dashed line) worsens the agreement with the experimental results.

For device simulations  $\mathbf{k} \cdot \mathbf{p}$  models have been well established. However, so far most of the parameters entering the  $\mathbf{k} \cdot \mathbf{p}$  Hamiltonian [30, 31] for GaN and InN have not been conclusively determined by experiment [2]. We

have therefore used our quasiparticle band structure to derive a complete set of Luttinger and  $A$ -parameters for zinc blende and wurtzite InN and GaN [32]. The parameters [29] are shown in Tab. II.

In conclusion, we have carried out  $G_0W_0$  band structure calculations based on exact-exchange density functional theory for InN and GaN. From these results we have derived key electronic quantities (band gaps, carrier dependence of the effective mass,  $\mathbf{k} \cdot \mathbf{p}$  parameters). For InN, a band gap of  $\approx 0.7$  eV is found supporting recent experimental observations. For all investigated parameters an excellent agreement with experimental data has been observed, indicating that the wide interval of experimentally observed band gaps can be largely explained by the Burnstein-Moss effect.

We would like to acknowledge fruitful discussions with Peter Kratzer, Matthias Wahn and Christoph Freysoldt. This work was in part supported by the Volkswagen Stiftung/Germany, the DFG through Sfb 296 and the research group „nitride based nanostructures” and the EU’s 6th Framework Programme through the NANOQUANTA (NMP4-CT-2004-500198) and SANDiE (NMP4-CT-2004-500101) Networks of Excellence.

- 
- [1] W. Walukiewicz, J. W. Ager III, K. M. Yu, Z. Lilienthal-Weber, J. Wu, S. X. Li, R. E. Jones, and J. D. Denlinger, J. Phys. D: Appl. Phys. **39**, R83 (2006).
  - [2] I. Vurgaftman and J. R. Meyer, J. Appl. Phys. **94**, 3675 (2003).
  - [3] V. Y. Davydov, A. A. Klochikhin, R. P. Seisyan, V. V. Emtsev, S. Ivanov, F. Bechstedt, J. Furthmüller, H. Harima, A. V. Mudryi, J. Aderhold, et al., phys. stat. sol. (b) **229**, R1 (2002).
  - [4] J. Wu, W. Walukiewicz, K. M. Yu, J. W. Ager III, E. E. Haller, H. Lu, W. Schaff, Y. Saiton, and Y. Nanishi, Appl. Phys. Lett. **80**, 3967 (2002).
  - [5] Y. Nanishi, Y. Saito, and T. Yamaguchi, Japan. J. Appl. Phys. **42**, 2549 (2003).
  - [6] A. Sher, M. van Schilfgaarde, M. A. Berding, S. Krishnamurthy, and A.-B. Chen, MRS Internet J. Nitride Semicond. Res. **4S1**, G5.1 (1999).
  - [7] F. Bechstedt and J. Furthmüller, J. Cryst. Growth **246**, 315 (2002).
  - [8] K. S. A. Butcher and T. L. Tansley, Superlattices and Microstructures **38**, 1 (2005).
  - [9] L. Hedin, Phys. Rev. **139**, A796 (1965).
  - [10] G. Onida, L. Reining, and A. Rubio, Rev. Mod. Phys. **74**, 601 (2002).
  - [11] P. Rinke, A. Qteish, J. Neugebauer, C. Freysoldt, and M. Scheffler, New J. Phys. **7**, 126 (2005).
  - [12] M. Usuda, N. Hamada, K. Shiraishi, and A. Oshiyama, Jpn. J. Appl. Phys. **43**, L407 (2004).
  - [13] T. Kotani and M. van Schilfgaarde, Solid State Commun. **121**, 461 (2002).
  - [14] A. Qteish, A. I. Al-Sharif, M. Fuchs, M. Scheffler, S. Boeck, and J. Neugebauer, Phys. Rev. B **72**, 155317 (2005).
  - [15] C. Stampfl, C. G. Van de Walle, D. Vogel, P. Krüger, and J. Pollmann, Phys. Rev. B **61**, R7846 (2000).
  - [16] D. Vogel, P. Krüger, and J. Pollmann, Phys. Rev. B **55**, 12836 (1997).
  - [17] J. Furthmüller, P. H. Hahn, F. Fuchs, and F. Bechstedt, Phys. Rev. B **72**, 205106 (2005).
  - [18] <http://www.sfhingx.de>.
  - [19] H. N. Rojas, R. W. Godby, and R. J. Needs, Phys. Rev. Lett. **74**, 1827 (1995).
  - [20] M. M. Rieger, L. Steinbeck, I. White, H. Rojas, and R. Godby, Comput. Phys. Commun. **117**, 211 (1999).
  - [21] L. Steinbeck, A. Rubio, L. Reining, M. Torrent, I. White, and R. Godby, Comput. Phys. Commun. **125**, 105 (2000).
  - [22] M. Moukara, M. Städele, J. A. Majewski, P. Vogl, and A. Görling, J. Phys. Condens. Matter **12**, 6783 (2000).
  - [23] For the wurtzite phases the internal lattice parameter  $u$  was determined by minimising the total energy in the LDA at fixed lattice constants  $a_0$  and  $c_0$ .
  - [24] C. Stampfl and C. G. V. de Walle, Phys. Rev. B **59**, 5521

- (1999).
- [25] J. Wu, W. Walukiewicz, W. Shan, K. M. Yu, J. W. Ager III, E. E. Haller, H. Lu, and W. Schaff, Phys. Rev. B **66**, 201403 (2002).
  - [26] W. Walukiewicz, S. X. Li, J. Wu, K. M. Yu, J. W. Ager III, E. E. Haller, H. Lu, and W. Schaff, J. Cryst. Growth **269**, 119 (2004).
  - [27] M. Losurdo, G. Bruno, T.-H. Kim, S. Choi, and A. Brown, Appl. Phys. Lett. **88**, 121928 (2006).
  - [28] V. A. Tyagai, A. M. Evstigneev, A. N. Krasiko, A. F. Andreeva, and V. Y. Malakhov, Sov. Phys. Semicond. **11**, 1257 (1977).
  - [29] Note that Eq. 1 results from a simplification of the  $\mathbf{k}\cdot\mathbf{p}$  Hamiltonian used for fitting the  $A$ -parameters. Therefore the values for  $E_p$  differ from Fig. 1 to Tab. II.
  - [30] E. O. Kane, Energy Band Theory, in Handbook on Semiconductors, vol. 1, W. Paul, Ed. Amsterdam, North Holland, 1982, pp. 193-217.
  - [31] S. L. Chuang and C. S. Chang, Phys. Rev. B **54**, 2491 (1996).
  - [32] The fit is not restricted to parabolic bands and  $E_p^\perp$  and  $E_p^\parallel$  are determined independently. Details of the procedure will be published elsewhere.